Comparing the Mechanical Response of Di-, Tri-, and Tetra-functional Resin Epoxies with Reactive Molecular Dynamics

M.S. Radue[1], Benjamin D. Jensen[1,2], S. Gowtham[1], D.R. Klimek-McDonald[1], J.A. King[1], G.M. Odegard[1]

[1] Michigan Technological University, Houghton, MI 49931
[2] NASA Langley Research Center, Hampton, VA 23666

ABSTRACT

The influence of monomer functionality on the mechanical properties of epoxies is studied using Molecular Dynamics (MD) with the Reax Force Field (ReaxFF). From deformation simulations, the Young's modulus, yield point, and Poisson's ratio are calculated and analyzed. The results demonstrate an increase in stiffness and yield strength with increasing resin functionality. Comparison between the network structures of distinct epoxies is further advanced by the Monomeric Degree Index (MDI). Experimental validation demonstrates the MD results correctly predict the relationship in Young's moduli. Therefore, ReaxFF is confirmed to be a useful tool for studying the mechanical behavior of epoxies.

INTRODUCTION

Epoxies are highly processable materials with excellent chemical and electrical resistance, high glass transition temperatures, and excellent adhesion properties relative to other polymer systems. When reinforced with high-strength fibers, epoxy-matrix composites provide great stiffness and strength while maintaining a relatively low weight. Thus, epoxy-matrix composites are increasingly being investigated and implemented in next-generation aircraft to replace metals used in major structural parts, such as wings and fuselages. The result is increased fuel efficiency and consequently lower emissions. Furthermore, in seeking improvement of the thermal conductivity and mechanical properties of epoxies, efforts have extended to incorporating various nanofillers. As epoxies continue to be valuable in fiber composites and nanocomposites, understanding the molecular behavior of epoxies remains critical. Developing and elucidating structure-property relationships in epoxies themselves may propel composite design on multiple scales. One such important structural feature to consider is the functionality of each monomer, that is, the number of monomers that can potentially be covalently bonded to a given monomer.

Experimental studies that have compared the mechanical properties of epoxies while varying the functionality of either the resin or hardener have shown mixed results. In a study from Becker et al., the pure epoxy results suggest an increase in flexural modulus with an increase in the functionality of the resin [1]. However, other studies do not yield a lucid link between the modulus or yield strength and the monomer functionality [2-4]. Differences in crosslink density or differences in other features of the monomer structure may obscure the effect of functionality. Early efforts to understand the mechanical response of polymers by rubber elasticity theory focused attention on the role of functionality. Crawford and Lesser later applied this theory to epoxies showing how the rubbery

moduli and the compressive yield stress relate to the functionality and the molecular weight between crosslinks [5].

Molecular Dynamics (MD) can be used to analyze epoxies on the nanometer length-scale in order to understand the influence of molecular structure on thermo-mechanical properties. Using MD the mechanical response of epoxies has been predicted with respect to system size [6] , mass ratio of resin to hardener molecules [7], strain rate [8-10], moisture content [11], and temperature [9-12]. Additionally, many MD studies have also considered the effect of crosslink density on the mechanical properties of epoxies, and it is clear that the stiffness increases with an increasing number of crosslinks [6, 10-16]. However, fewer MD studies have tackled the role of functionality on the stress-strain response [17-19]. Among these studies, Tsige et al. implemented a coarse-grained model with two potential terms and showed the yield strength, ultimate strength, and strain at failure to depend on functionality [19]. Particularly, the yield strength was shown to increase with increasing functionality. Li et al. undertook a more detailed MD approach by modeling a specific epoxy resin with various hardeners containing either two or three amine groups [17]. However, no all-atom modeling study has thoroughly compared the elastic properties and yielding characteristics for different epoxies having at least three unique combinations of monomer functionalities.

The goal of this study is to predict the mechanical properties of a di-functional, tri-functional, and tetra-functional resin epoxy using MD. The deformation of multiple crosslinked samples of each epoxy type were simulated using a reactive force field. The corresponding Young's modulus, Poisson's ratio, and yield point were predicted and compared. Additionally, the effect of network characteristics on these properties were analyzed. For model validation, the predicted mechanical properties were compared to experimentally-obtained values obtained herein, as well as literature values.

MOLECULAR MODELING

To simulate the levels of strain associated with the bulk failure of epoxies, it is expected that covalent bonds will be stretched beyond the distances for which traditional fixed-bond force fields are characterized. Additionally, most fixed-bond MD force fields are not developed to predict changes in bond configuration. ReaxFF can capture large magnitudes of stretching and simulate the creation and scission of covalent bonds by assigning a bond order (1 for single bond, 2 for double bond, etc.) for all relevant pairs of atoms based on the interatomic distance. The corresponding interatomic forces are determined based on the bond order, and the bond orders are updated throughout a simulation allowing for the creation and breaking of bonds. All parameters used by ReaxFF are optimized *a priori* to reproduce results from quantum mechanics computations for select, small molecular systems.

In this work, the reactive force field ReaxFF [20] with the low-gradient corrected parameters of Liu *et al*. [21] were selected and implemented using LAMMPS [22, 23]. The development of the Liu *et al.* parameter set traces back to the original ReaxFF parameter set by van Duin *et al.* [20]. The original ReaxFF parameter set was parameterized to reproduce experimental heats of formation and bond and angle data for small hydrocarbons. Additionally, hydrocarbon bond dissociation curves and rotational energy barriers from quantum mechanics calculations were included for determining the parameters. Strachan *et al.* extended the original ReaxFF parameter set to include nitrogen and oxygen for studying the thermal decomposition of the energetic material RDX [24, 25]. The training set was expanded to include density functional theory (DFT) bond dissociation, angle bending, and torsion rotation energies for a variety of CHNO molecules. The Strachan *et al.* parameter set served as the basis of the Liu *et al.* parameter set. Liu *et al*. added a new ReaxFF energy term to improve the

accuracy of long-range van der Vaals interactions for molecular solids [21]. The correction parameters were designed to reproduce the experimental heats of formation and densities of the crystal structures of graphite, polyethene, carbon dioxide, solid nitrogen, and energetic materials. The Liu *et al*. parameter set was selected since it contains the required elements for modeling epoxide and amine groups, demonstrates improved van der Waals interactions for solids, and has been shown to provide reliable results for determining elastic moduli and the yield point of epoxies [8].

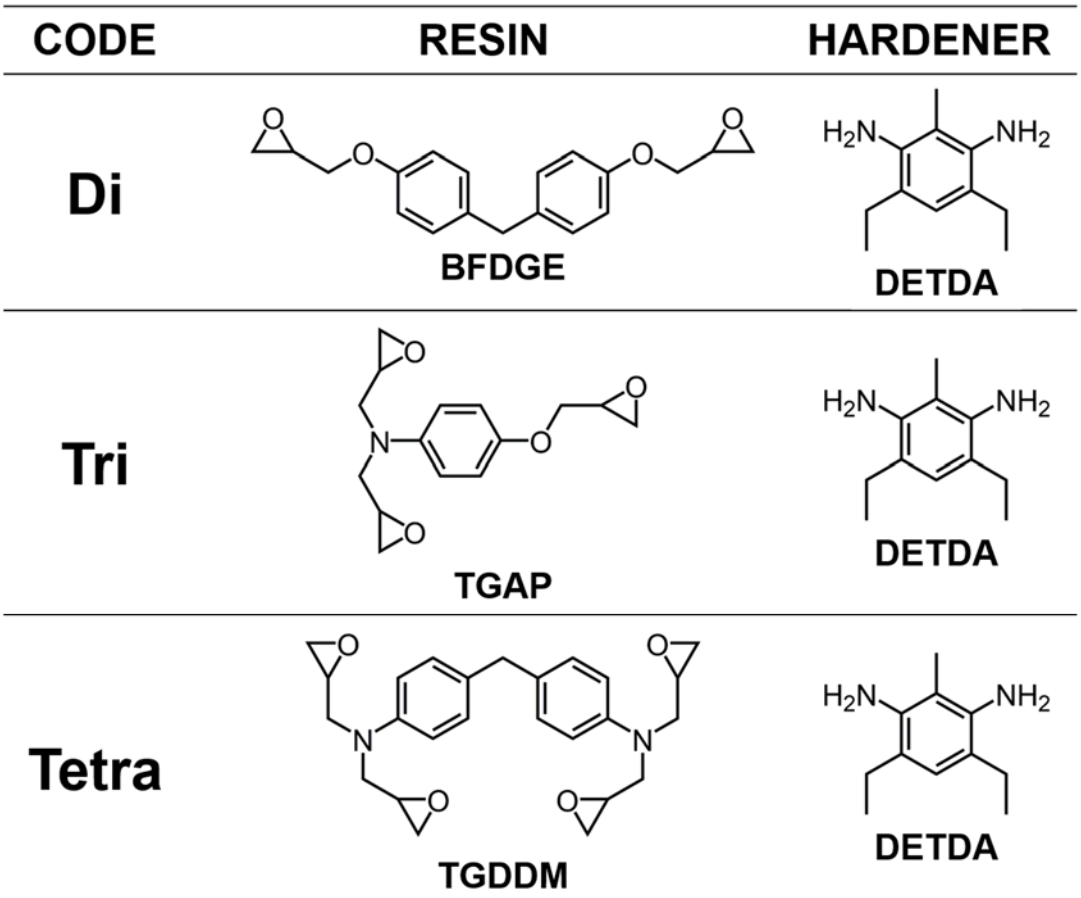

Figure 1. Epoxy systems modeled and the skeletal structures of the resin and hardener monomers

The resin molecules chosen were bisphenol F diglycidyl ether (BFDGE, EPON 862), tri-glycidyl para-amino phenol (TGAP, Araldite MY 0510), and tetra-glycidyl-4,4'-diaminodiphenylmethane (TGDDM, Araldite MY 721). One hardener was used, namely, diethyltoluenediamine (DETDA). Using these resins and hardener, three different epoxy systems were composed: BFDGE/DETDA, TGAP/DETDA, and TGDDM/DETDA. The epoxy systems modeled and the molecular structures of the monomers are shown in Figure 1. The functionality of the resin monomers is determined by the number of epoxide groups. The number of epoxide groups of BFDGE, TGAP, and TGDDM are 2, 3, and 4 respectively, which is the key distinguishing factor between each epoxy. Thus, the names Di, Tri, and Tetra refer to the epoxies BFDGE/DETDA, TGAP/DETDA, and TGDDM/DETDA, respectively, as indicated in Figure 1. Each amine group can react with two epoxide groups during crosslinking. Thus, the ratio of resin monomers to hardener monomers was chosen so that exactly two epoxide groups were present for every amine group. For the di-, tri-, and tetra-functional resin epoxies,

the ratio of resin to hardener molecules was 2:1, 4:3, and 1:1 respectively. Table I gives the resin functionality f_r, the number of resin and hardener molecules, and the total number of atoms for each epoxy model.

TABLE I. MODELING DETAILS FOR EACH EPOXY TYPE

EPOXY	f_r	NO. OF RESINS	NO. OF HARDENERS	RESIN TO HARDENER RATIO	TOTAL NO. OF ATOMS
Di	2	90	45	2:1	5265
Tri	3	84	63	4:3	5229
Tetra	4	57	57	1:1	5244

To perform the epoxide-amine crosslinking reactions, high-energy bonds were created as an initial step. To ensure that the epoxy molecular structure is not inadvertently damaged upon network formation, all epoxy models were initially built using the OPLS all-atom force field [26]. Since OPLS is a fixed-bond force field, all other bonds will remain intact when large energy spikes are introduced in the system. It is expected that creating high-energy bonds in ReaxFF would result in unintended dissociation of neighboring bonds.

First, the monomers were arrayed sparsely in a periodic simulation box. The initial mass densities were in the range of 0.09-0.10 g/cm^3. A fixed-volume simulation of 100 ps was performed to allow the monomers to mix, in which the temperature was gradually ramped down from 600 K to 300 K. For each epoxy system, five independent uncrosslinked samples were generated. To ensure the uniqueness of each sample, different initial velocities were assigned for each sample prior to the mixing process. Following these mixing simulations, the simulation boxes were slowly compressed to densities of 1.21 g/cm^3. These simulations occurred at 300 K for a total of 4 ns, and 20 molecular minimizations were performed at regular intervals during the process.

The monomers were crosslinked by executing the epoxide-amine reactions shown in Figure 2. Reaction 1 shows one epoxide group and a primary amine reacting to open the epoxide ring and form a hydroxyl group and a secondary amine. Moreover, the secondary amine can proceed to react with another epoxide group (Reaction 2) forming a tertiary amine and another hydroxyl group. These reactions were accomplished using a series of LAMMPS commands including ‘fix bond/create’ and ‘fix bond/break’. An eligible reaction occurred when a carbon in an epoxide group and a nitrogen in an amine group were at a distance of 7 angstroms or less. Each eligible reaction was randomly confirmed to react. The approved reactions proceeded by applying a harmonic bond potential between the C and N. The C-O epoxide bond and one N-H amine bond were subsequently broken, and a new hydroxyl group was created. In order to help bring newly created bonds close to their equilibrium distance, the Langevin thermostat was used [27, 28] along with the ‘fix nve/limit’ command which places an upper bound on the distance an atom can move in a single time step. The crosslinking process was carried out for up to 1 ns. For some monomer samples, multiple crosslinked models were created by executing the crosslinking process for varying durations. Upon crosslinking, no angles or dihedrals were added since the models would later be simulated with ReaxFF, which independently accounts for the angles and dihedrals.

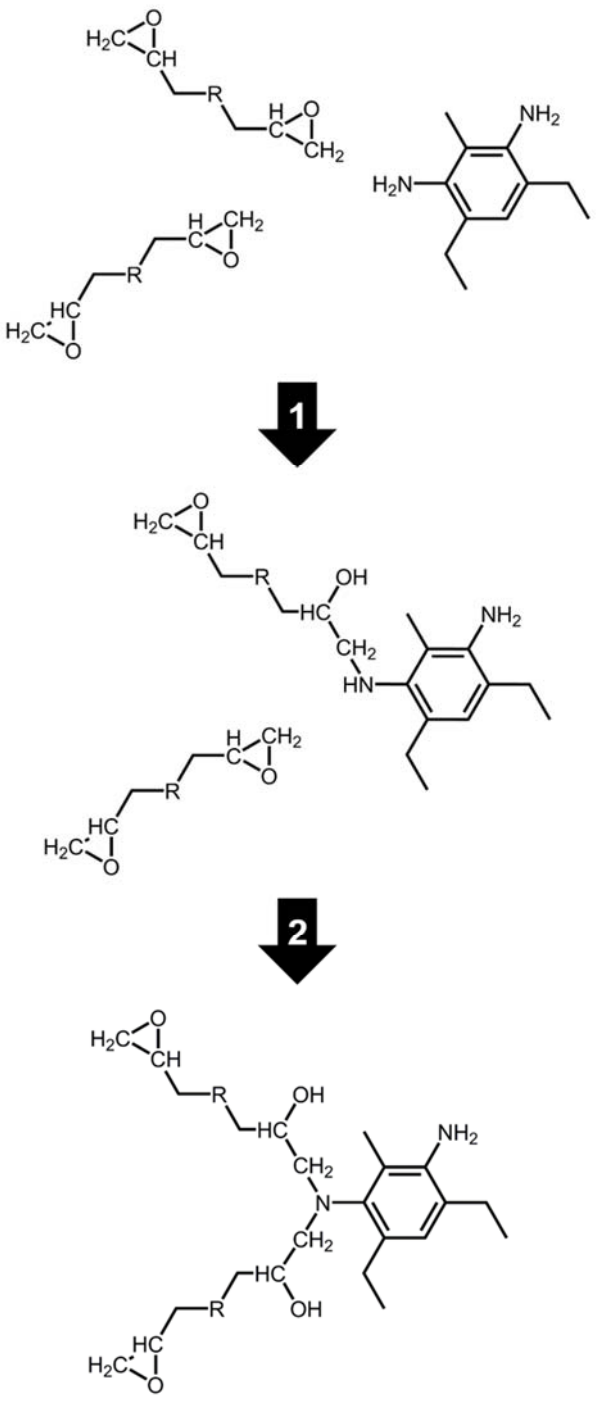

Figure 2. Epoxide-amine crosslinking reactions.

The monomeric degree index (MDI) was defined as the average number of monomeric units that are covalently bonded to a given monomeric unit. This average is taken over all monomeric units in the MD model. A simple oligomer example is shown in Figure 3 where the number of bonded units is denoted. Averaging over all resins and hardeners, the MDI is about 1.67, that is, on average a monomer unit is bonded to 1.67 units. The crosslink density can also be determined for this example. The crosslink density can be defined as the number of reactions performed during crosslinking

divided by the maximum number of theoretically possible reactions. In this example, 5 bonds are formed out of a total of 8 possible bonds giving a crosslink density of 0.625.

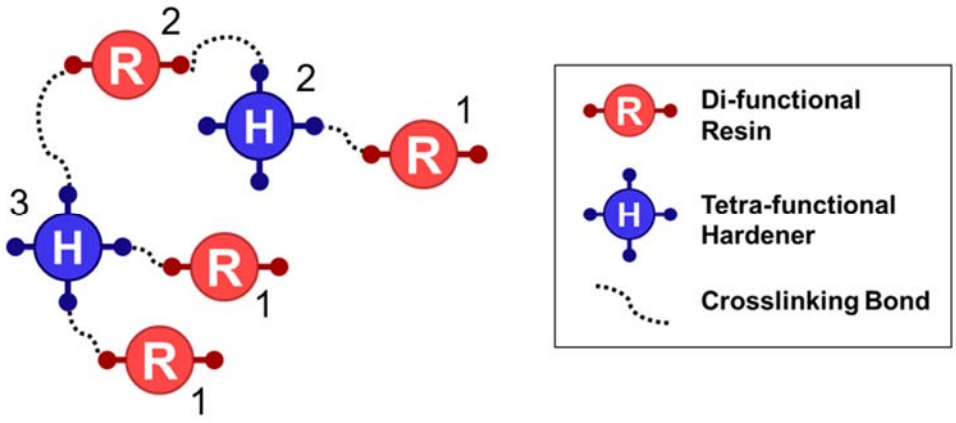

Figure 3. Oligomer example with the number of bonded units indicated for each monomeric unit

Two purposes are served by introducing the MDI. First, the MDI elucidates the nature of network junctions in the epoxy models. The usual measure of functionality describes the *potential* number of monomeric units that can be bonded to a given monomeric unit. However, during the MD crosslinking procedure, not all reactive sites will engage in a reaction; e.g., a monomer that is capable of covalently bonding to four monomers may only bond to two or three monomers. Thus, the MDI is chosen to describe the network structure in light of incomplete bonding. Secondly, the MDI serves as an alternative to the crosslink density to measure the degree of cure. The crosslink density is defined using the maximum number of theoretically possible reactions, which differs between the epoxies studied here. Because the MDI is independent of the number of theoretically possible reactions, it is more suitable than the crosslink density for comparing dissimilar epoxies.

The MDI values and crosslink densities of all models are shown in Table II. Five models for each epoxy type are highlighted as *characteristically crosslinked*. A range of experimental crosslink densities of 60%-95% is typically observed for epoxies [29-32]. The characteristically crosslinked models possess crosslink densities of about 70%-85%, placing these models in the middle of the experiment range. The five characteristically crosslinked models were selected for predicting the mechanical properties of each epoxy. The remaining low crosslinked models were developed as supplemental models to establish the MDI-property relationships described below.

As expected, the Di model is not capable of attaining high MDIs relative to the other epoxies, and the Tetra model produces the greatest MDI values. For each epoxy type, a range of MDIs were generated from about 1.5 to the maximum value. Fewer Di models than Tri or Tetra were required to span this range. Table II also shows that the characteristically crosslinked Tri models obtained the highest average crosslink density. The smaller size of TGAP (having one benzene ring instead of two as with BFDGE and TGDDM) is the suspected cause of the higher crosslinking percent.

TABLE II. MDI VALUES AND CROSSLINK DENSITIES OF ALL MODELS

EPOXY	CURE CATEGORY	MODEL NO.	MDI	CROSSLINK DENSITY
Di	Characteristic Crosslinking	1	2.27	0.85
		2	2.24	0.84
		3	2.19	0.82
		4	2.05	0.77
		5	1.89	0.71
	Low Crosslinking	6	1.54	0.58
		7	1.45	0.54
Tri	Characteristic Crosslinking	1	2.91	0.85
		2	2.88	0.84
		3	2.78	0.81
		4	2.78	0.81
		5	2.67	0.78
	Low Crosslinking	6	2.52	0.73
		7	2.48	0.72
		8	1.93	0.56
		9	1.88	0.55
		10	1.56	0.46
		11	1.48	0.43
Tetra	Characteristic Crosslinking	1	3.20	0.80
		2	3.16	0.79
		3	3.12	0.78
		4	3.00	0.75
		5	2.88	0.72
	Low Crosslinking	6	2.62	0.65
		7	2.53	0.63
		8	2.33	0.58
		9	2.21	0.55
		10	1.90	0.47
		11	1.76	0.44

The crosslinked models were switched from OPLS to ReaxFF with the parameter set containing low gradient corrections developed by Liu *et al.* [21]. The above-described procedure of neglecting the angle and dihedral parameters associated with the newly formed crosslinks caused some hydroxyl groups to dissociate in ReaxFF. However, this was rectified by a 100 ps simulation where all atoms were frozen except the hydroxyl group hydrogens, which were limited in kinetic energy by the 'temp/rescale' and 'fix viscous' commands. This allowed ReaxFF to correct the C-O-H angles. Afterwards, all atoms were gradually brought into motion by ramping the temperature from 1 K to 300 K over 100 ps.

Equilibration occurred over 1.5 ns at 300 K. Using the NPT ensemble, the Nose-Hoover barostat was set to maintain 1 atm of pressure on all sides of the simulation box. A timestep of 0.1 fs was used. Table III provides the average mass density after equilibration for the characteristically crosslinked models. All uncertainty measures used in this paper indicate the standard deviation. The model densities are compared with experimental measurements in Table III showing good agreement.

After establishing the equilibrated models, each model was subjected to three uniaxial tensile deformation simulations: tension in the x- , y- , and z- directions. Deformations were performed every timestep amounting to 20% engineering strain over 1 ns, resulting in a strain rate of 2×10^{8} s^{-1}. In the transverse directions, the Nose-Hoover barostat was assigned to maintain 1 atm of pressure to enable Poisson contractions. A timestep of 0.1 fs and a temperature of 300 K was specified.

TABLE III. COMPARISON OF MASS DENSITIES

EPOXY	MODEL DENSITY g/cm^3	EXPERIMENTAL DENSITY g/cm^3
Di	1.222 ± 0.005	1.20 [33]
Tri	1.235 ± 0.011	1.24 [1]
Tetra	1.221 ± 0.002	1.20 [1]

SPECIMEN FABRICATION AND TESTING

Experimental samples of the tetra-functional resin epoxy, TGDDM/DETDA, were prepared to aid in the validation of the MD model. The resin used was Araldite® MY721 (TGDDM), and Aradur® 5200 was used for the DETDA hardener. Both the resin and hardener were obtained from Huntsman. The epoxy was prepared by first placing 100g of TGDDM and 35g of DETDA into separate beakers. The beaker of TGDDM resin was placed in a water bath at 50 °C to lower the viscosity. While in the water bath, the resin was stirred using a Ross High Shear Mixer (HSM-100 LSKI) with 2 inch dispersion blade. The mixer was set to the lowest speed (~500 rpm) and the DETDA hardener was then slowly poured into the TGDDM resin. The mixture was mixed at 500 rpm for 10 min until the two parts were thoroughly mixed. The mixture was then degassed at 70 °C and 29 inHg with alternating vacuum to avoid overflow until no additional bubbles appeared. The mixture was then poured into a preheated (70 °C) multi-part mold that had been coated with Mann Ease Release 300 and degassed a final time. The curing cycle used was 150 °C for two hours, then heated to 180 °C at a rate of 2 °C/min, and held at 180 °C for two hours. The oven was then turned off, and the cured epoxy was allowed to cool in the oven to room temperature, which resulted in a cooling rate of approximately 1 °C/min.

The Young's moduli of ten epoxy samples were determined at ambient conditions according to ASTM D638 at a crosshead rate of 1 mm/min. The test specimens were ASTM Type I sample geometry: 165 mm long and 3.3 mm thick. The samples were tested using an InstruMet Sintech screw-driven mechanical testing machine. Stress values were recorded by the testing machine, and an extensometer was used to collect strains. Samples were conditioned at 23 °C and 50% relative humidity for 2 days prior to testing.

RESULTS

Stress-strain curves were analyzed for each MD deformation simulation. The true stress and true strain were calculated in the axial direction. To obtain the Young's modulus, the stress-strain data was fit with a linear regression model for strains up to about 3%. A moving average was calculated to smooth the scattered stress-strain data typical of MD models at finite temperatures [8]. The smoothing allowed for a more precise determination of the yield point. The yield point was defined as the location where the smoothed stress-strain curve crossed the 0.2% offset line. A representative stress-strain plot with a linear fit for small strains, the 0.2% offset line, and the smoothed curve is shown in Figure 4.

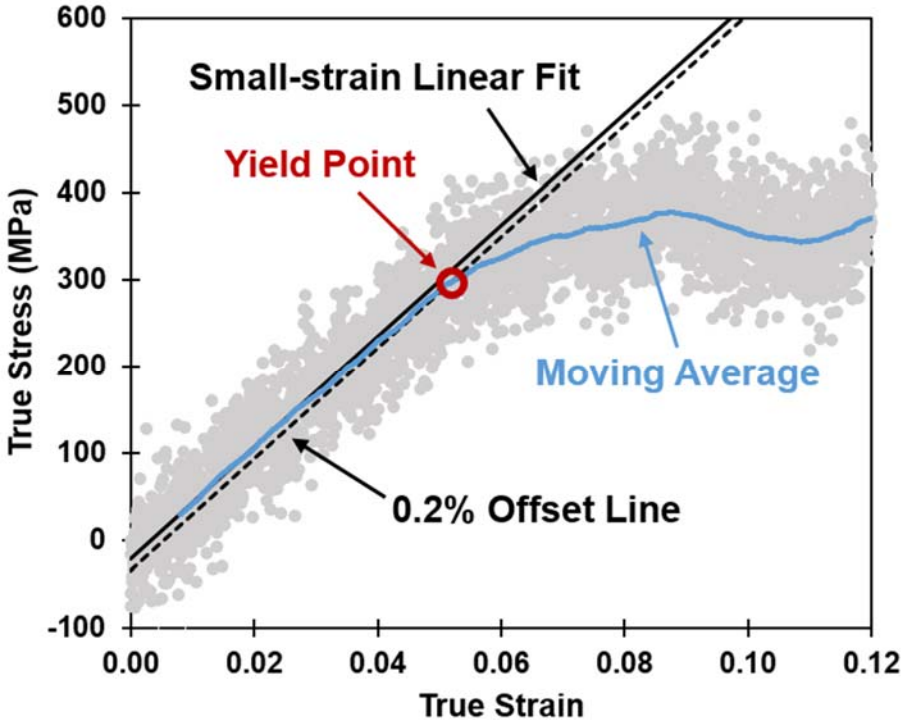

Figure 4. Representative stress-strain curve from MD simulation

The predicted Young's moduli from the MD simulations are shown in Table IV for all three epoxy systems. The corresponding uncertainties represent the standard deviation between the five characteristically crosslinked models. Also shown in Table IV are the measured Young's moduli from the above-described experimental tests on the tetra-functional epoxy, as well as the literature value for the di-functional epoxy from Littell *et al.* [34]. No literature results for the Young's modulus of the tri-functional resin epoxy could be found since TGAP is commonly cured with 4,4'-diaminodiphenyl sulfone (DDS) rather than DETDA. For both the Di and Tetra epoxies, the values obtained from simulation overpredict the measured value. This can be explained by the stiffening effect of high strain rates that is observed experimentally [8, 34, 35].

Figure 5 shows the Young's modulus of the di-functional system as a function of strain rate from experimental measurements by Littell *et al.* [34] and from the present MD modeling. Notice that there is a significant gap between the experimental and computational strain rates. Typical high strain rate testing is performed using the Split Hopkinson Pressure Bar (SHPB) which reaches to the order of 10^3 s^{-1}. However, due the computational demand of MD, mechanical deformation simulations are limited to even higher strain rates. Currently, it is yet unfeasible for MD simulations to reach the strain rates of the SHPB test. It remains to be seen how experimental and MD mechanical data for epoxies compare at matching strain rates. Nevertheless, Figure 5 indicates that the MD prediction generally follows the experimentally set trend.

In spite of the difference in strain rate, the MD simulations correctly predict that the Tetra epoxy is stiffer than the Di epoxy (Table IV). Additionally, the molecular modeling of the tri-functional resin epoxy predicts that the Young's modulus will fall between the di- and tetra-functional resin epoxies. The experimentally measured flexural moduli from Becker *et al.* [1, 36] and Zhou *et al.* [37] are also shown in Table IV for validation of this trend. For the three epoxy systems studied, the Young's modulus appears to increase with increasing resin functionality.

TABLE IV. COMPARISION OF ELASTIC MODULI RESULTS

EPOXY	YOUNG'S MODULUS FROM SIMULATION GPa	YOUNG'S MODULUS FROM EXPERIMENT GPa	FLEXURAL MODULUS FROM EXPERIMENT GPa
Di	3.51 ± 0.72	2.89 [34]	2.46 [37]
Tri	4.94 ± 0.98	--	2.76 ± 0.14 [1, 38]
Tetra	5.30 ± 0.81	3.39 ± 0.11*	3.04 ± 0.04 [1, 38]

* Young's modulus for the Tetra epoxy was obtained in this work

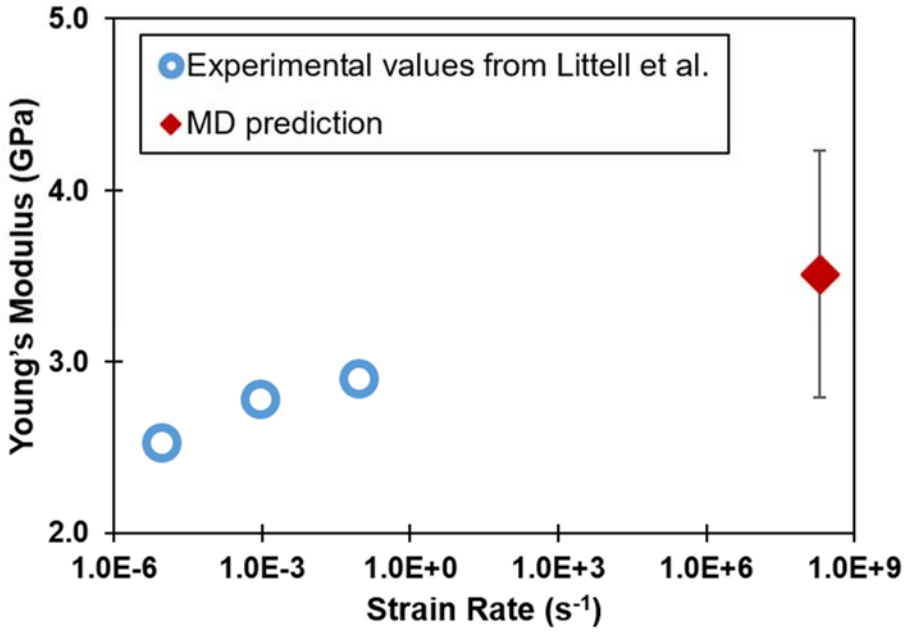

Figure 5. Young's modulus versus strain rate for experimental [34] and predicted results for BFDGE/DETDA.

The average MDIs for the characteristically crosslinked di-, tri-, and tetra-functional resin epoxies were 2.1, 2.8, and 3.1 respectively. The Tri systems have MDIs that are closer to the Tetra models than the Di models due to the higher crosslink densities obtained by the Tri models. Similarly, Table IV indicates that the difference between the average moduli for the Tetra and Tri models (0.36 GPa) is less than the difference between the Tri and Di models (1.43 GPa). While this is not observed for the flexural moduli obtained by Becker *et al.* [1, 38], this could be due to differences in the extent of crosslinking which was not identified in the study. For the MD models simulated here, the MDI suggests that the highly crosslinked Tri networks resemble the Tetra networks which is evidenced by the similar Young's moduli.

In Figure 6, the Young's modulus is plotted with respect to the MDI for all models. Each data point indicates the mean Young's modulus of one model, and the standard deviation is shown from three uniaxial tensile simulations. In general, there appears to be a trend of increasing Young's modulus with increasing MDI for all models. However, it is difficult to discern the precise nature of this trend due to the uncertainties observed for these MD models. To elaborate on the observed trend consider the various Tetra models. The low-crosslinked Tetra models with MDIs of 1.9, 2.2, and 2.3 provided mean Young's modulus values of 3.70, 4.00, and 3.61 GPa respectively. The stiffnesses of the low-crosslinked Tetra models are unlike those observed for the high-crosslinked Tetra models (5.30 ± 0.81 GPa). However, these low-crosslinked Tetra models have similar MDI values as the

high-crosslinked Di models. Unsurprisingly, these low-crosslinked Tetra models possess similar Young's moduli as the high-crosslinked Di models (3.51 ± 0.72 GPa).

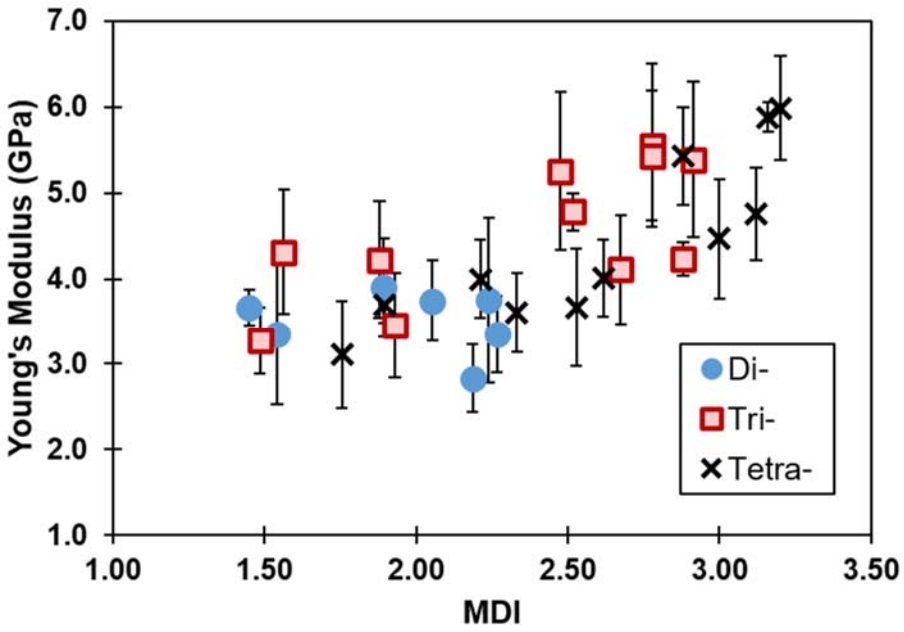

Figure 6. Young's modulus versus MDI for all epoxy models.

The yield stress and yield strain results are given in Table V. The yield stress is shown to increase with increasing resin functionality which agrees with previous MD results [19]. Comparing the yield stress to experimental results is challenging since the yield stress is known to be especially sensitive to strain rate [34, 35]. Figure 7 shows the experimental yield stress results for the di-functional resin system [34] using various strain rates and the predicted MD results from this study. It is observed from experimental results that the yield stress increases with increasing strain rate. Thus, it is expected that the values obtained from MD simulation should indeed be higher than experimental measurements.

Figure 8 shows the yield stress versus MDI for all models. Each data point indicates the average yield stress from deforming an individual epoxy model in three directions. Figure 8 suggests a trend of increasing yield stress with increasing MDI. The yield strain was consistent for all three epoxy types modeled, and no noticeable effect of the MDI on the yield strain was observed.

TABLE V. YIELD POINT RESULTS FROM SIMULATION

EPOXY	YIELD STRESS MPa	YIELD STRAIN
Di	135 ± 36	0.039 ± 0.011
Tri	187 ± 58	0.039 ± 0.011
Tetra	196 ± 50	0.037 ± 0.009

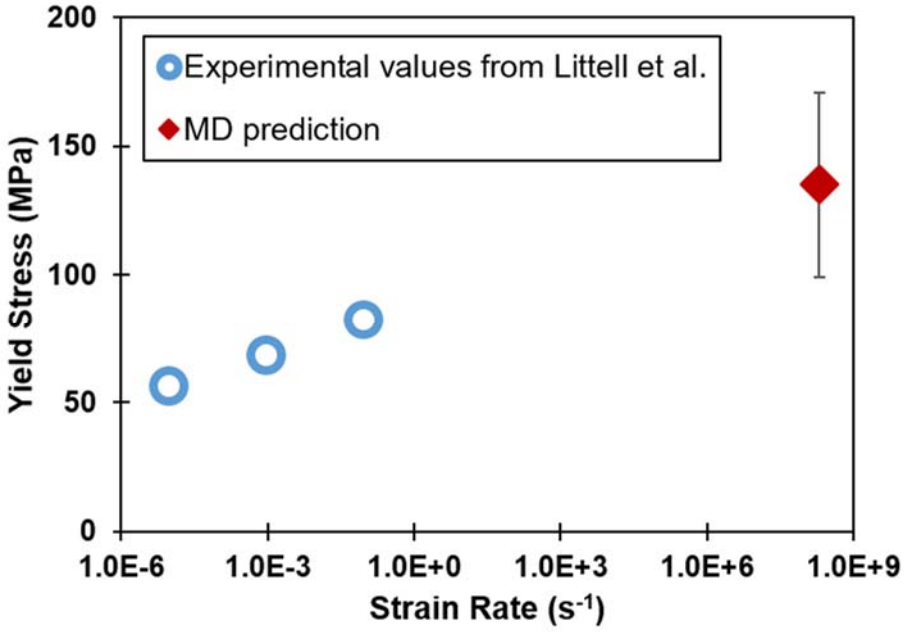

Figure 7. Yield stress versus strain rate for experimental [34] and predicted results for BFDGE/DETDA.

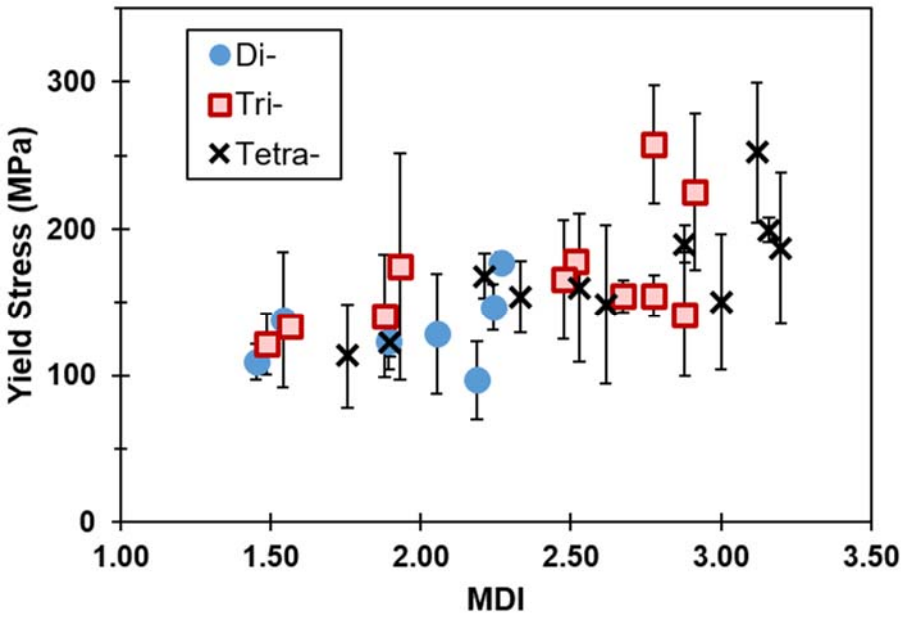

Figure 8. Yield stress versus MDI results for all epoxy models.

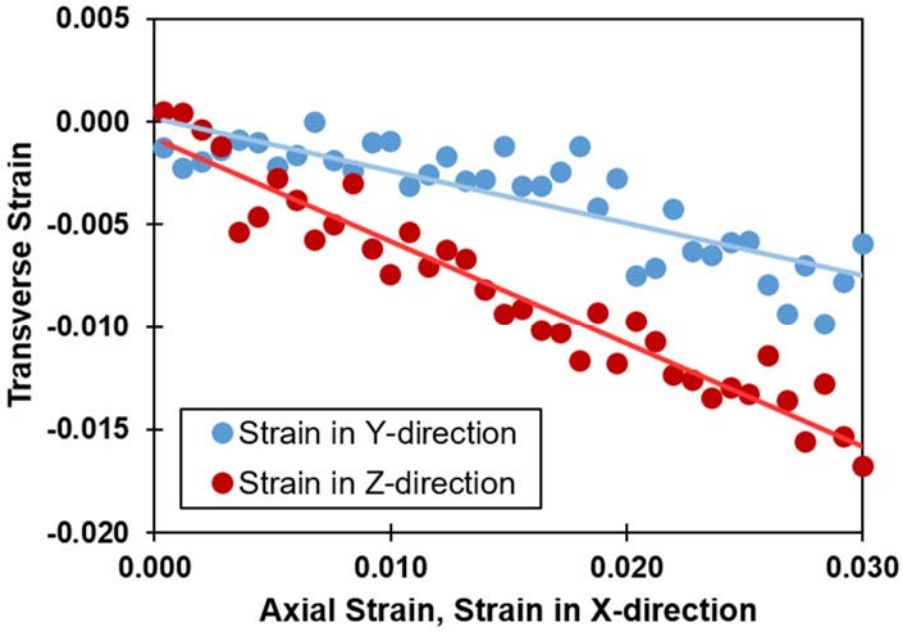

Figure 9. Representative transverse strain versus axial strain plot with linear fit.

The Poisson's ratio was determined from the transverse strain versus axial strain plots as shown in Figure 9. A linear fit of for both transverse directions was determined. The negative of the slope of each line was averaged together to get the Poisson's ratio. Table VI gives the Poisson's ratio for each epoxy type. For the di-functional resin epoxy, the Poisson's ratio obtained from experiments were in the range of 0.40-0.43 [34]. The MD simulations give the Poisson's ratio to be 0.37 ± 0.05 showing reasonable agreement with experiment considering the Poisson's ratio is independent of strain rate for epoxy [34].

TABLE VI. POISSON'S RATIO RESULTS FROM SIMULATION

EPOXY	POISSON'S RATIO
Di	0.37 ± 0.05
Tri	0.37 ± 0.03
Tetra	0.35 ± 0.04

CONCLUSIONS

The results of this study indicate that the monomer functionality has a significant influence on the Young's modulus and yield stress. Both the Young's modulus and yield stress increased with increasing resin functionality. The experimental literature results reveal the mechanical property rate-dependence. While the difference between the simulation and experimental strain rates is considerable, the MD results generally follow the experimentally set trend. However, it remains challenging to accurately compare the MD mechanical predictions with quasi-static experimental results. Additional mechanical data at strain rates above 10 s^{-1} are desirable to better link experimental and computational results. The MD models correctly indicate the relative stiffness between the three epoxies studied. This further suggests that ReaxFF with the Liu *et al.* parameter set is valuable for predicting the stress-strain response of epoxies and understanding structure-property trends. The latter

is facilitated by the ability to fully define all details of an MD-modeled polymer network. We demonstrate how characterizing the network junctions allows for informative comparisons between three distinct epoxies by introducing the MDI. Aggregating the mechanical data for all epoxies modeled, the Young's modulus and yield stress is shown to generally increase with increasing MDI.

REFERENCES

1. Becker, O., R. Varley, and G. Simon, *Morphology, thermal relaxations and mechanical properties of layered silicate nanocomposites based upon high-functionality epoxy resins.* Polymer, 2002. **43**(16): p. 4365-4373.
2. Amaral, C.R., et al., *Impact of Aliphatic Amine Comonomers on DGEBA Epoxy Network Properties.* Polymer Engineering and Science, 2014. **54**(9): p. 2132-2138.
3. Garcia, F.G., et al., *Influence of Chemical Structure of Hardener on Mechanical and Adhesive Properties of Epoxy Polymers.* Journal of Applied Polymer Science, 2010. **117**(4): p. 2213-2219.
4. Grishchuk, S., et al., *Structure, thermal, and mechanical properties of DDM-hardened epoxy/benzoxazine hybrids: Effects of epoxy resin functionality and ETBN toughening.* Journal of Applied Polymer Science, 2013. **127**(6): p. 5082-5093.
5. Crawford, E. and A.J. Lesser, *The effect of network architecture on the thermal and mechanical behavior of epoxy resins.* Journal of Polymer Science Part B-Polymer Physics, 1998. **36**(8): p. 1371-1382.
6. Shenogina, N.B., et al., *Molecular Modeling Approach to Prediction of Thermo-Mechanical Behavior of Thermoset Polymer Networks.* Macromolecules, 2012. **45**(12): p. 5307-5315.
7. Nouri, N. and S. Ziaei-Rad, *A Molecular Dynamics Investigation on Mechanical Properties of Cross-Linked Polymer Networks.* Macromolecules, 2011. **44**(13): p. 5481-5489.
8. Odegard, G.M., et al., *Predicting mechanical response of crosslinked epoxy using ReaxFF.* Chemical Physics Letters, 2014. **591**: p. 175-178.
9. Sirk, T.W., et al., *High strain rate mechanical properties of a cross-linked epoxy across the glass transition.* Polymer, 2013. **54**(26): p. 7048-7057.
10. Yang, S. and J. Qu, *Computing thermomechanical properties of crosslinked epoxy by molecular dynamic simulations.* Polymer, 2012. **53**(21): p. 4806-4817.
11. Clancy, T.C., et al., *Molecular modeling for calculation of mechanical properties of epoxies with moisture ingress.* Polymer, 2009. **50**(12): p. 2736-2742.
12. Li, C. and A. Strachan, *Molecular dynamics predictions of thermal and mechanical properties of thermoset polymer EPON862/DETDA.* Polymer, 2011. **52**(13): p. 2920-2928.
13. Bandyopadhyay, A., et al., *Molecular modeling of crosslinked epoxy polymers: The effect of crosslink density on thermomechanical properties.* Polymer, 2011. **52**(11): p. 2445-2452.
14. Shenogina, N.B., et al., *Molecular modeling of elastic properties of thermosetting polymers using a dynamic deformation approach.* Polymer, 2013. **54**(13): p. 3370-3376.
15. Shokuhfar, A. and B. Arab, *The effect of cross linking density on the mechanical properties and structure of the epoxy polymers: molecular dynamics simulation.* Journal of Molecular Modeling, 2013. **19**(9): p. 3719-3731.
16. Bandyopadhyay, A. and G.M. Odegard, *Molecular modeling of crosslink distribution in epoxy polymers.* Modelling and Simulation in Materials Science and Engineering, 2012. **20**(4): p. 17.
17. Li, C., E. Coons, and A. Strachan, *Material property prediction of thermoset polymers by molecular dynamics simulations.* Acta Mechanica, 2014. **225**(4-5): p. 1187-1196.
18. Tsige, M., C.D. Lorenz, and M.J. Stevens, *Role of network connectivity on the mechanical properties of highly cross-linked polymers.* Macromolecules, 2004. **37**(22): p. 8466-8472.
19. Tsige, M. and M.J. Stevens, *Effect of cross-linker functionality on the adhesion of highly cross-linked polymer networks: A molecular dynamics study of epoxies.* Macromolecules, 2004. **37**(2): p. 630-637.
20. Van Duin, A.C., et al., *ReaxFF: a reactive force field for hydrocarbons.* The Journal of Physical Chemistry A, 2001. **105**(41): p. 9396-9409.
21. Liu, L.C., et al., *ReaxFF-/g: Correction of the ReaxFF Reactive Force Field for London Dispersion, with Applications to the Equations of State for Energetic Materials.* Journal of Physical Chemistry A, 2011. **115**(40): p. 11016-11022.
22. Plimpton, S., *Fast parallel algorithms for short-range molecular dynamics.* Journal of computational physics, 1995. **117**(1): p. 1-19.
23. Aktulga, H.M., et al., *Parallel reactive molecular dynamics: Numerical methods and algorithmic techniques.* Parallel Computing, 2012. **38**(4): p. 245-259.

24. Strachan, A., et al., *Shock waves in high-energy materials: The initial chemical events in nitramine RDX.* Physical Review Letters, 2003. **91**(9): p. 098301.
25. Strachan, A., et al., *Thermal decomposition of RDX from reactive molecular dynamics.* The Journal of chemical physics, 2005. **122**(5): p. 054502.
26. Jorgensen, W.L., D.S. Maxwell, and J. TiradoRives, *Development and testing of the OPLS all-atom force field on conformational energetics and properties of organic liquids.* Journal of the American Chemical Society, 1996. **118**(45): p. 11225-11236.
27. Schneider, T. and E. Stoll, *Molecular-dynamics study of a three-dimensional one-component model for distortive phase transitions.* Physical Review B, 1978. **17**(3): p. 1302.
28. Jensen, B.D., K.E. Wise, and G.M. Odegard, *The effect of time step, thermostat, and strain rate on ReaxFF simulations of mechanical failure in diamond, graphene, and carbon nanotube.* Journal of computational chemistry, 2015. **36**(21): p. 1587-1596.
29. Varley, R., et al., *Toughening of a trifunctional epoxy system: 1. Near infra-red spectroscopy study of homopolymer cure.* Polymer, 1995. **36**(7): p. 1347-1355.
30. Dannenberg, H. and W. Harp Jr, *Determination of cure and analysis of cured epoxy resins.* Analytical Chemistry, 1956. **28**(1): p. 86-90.
31. Musto, P., et al., *The curing process and moisture transport in a tetrafunctional epoxy resin as investigated by FT-NIR spectroscopy.* High Performance Polymers, 2000. **12**(1): p. 155-168.
32. Poisson, N., G. Lachenal, and H. Sautereau, *Near-and mid-infrared spectroscopy studies of an epoxy reactive system.* Vibrational spectroscopy, 1996. **12**(2): p. 237-247.
33. *Product Bulletin SC:1183-02*. 2001, Resolution Performance Products LLC.
34. Littell, J.D., et al., *Measurement of epoxy resin tension, compression, and shear stress-strain curves over a wide range of strain rates using small test specimens.* Journal of Aerospace Engineering, 2008. **21**(3): p. 162-173.
35. Buckley, C.P., et al., *Deformation of thermosetting resins at impact rates of strain. Part I: Experimental study.* Journal of the Mechanics and Physics of Solids, 2001. **49**(7): p. 1517-1538.
36. Lincoln, J.E., R.J. Morgan, and E.E. Shin, *Moisture absorption-network structure correlations in BMPM/DABPA bismaleimide composite matrices.* Journal of Advanced Materials, 2000. **32**(4): p. 24-34.
37. Zhou, Y., et al., *Experimental study on the thermal and mechanical properties of multi-walled carbon nanotube-reinforced epoxy.* Materials Science and Engineering: A, 2007. **452**: p. 657-664.
38. Becker, O., et al., *Layered silicate nanocomposites based on various high-functionality epoxy resins: The influence of cure temperature on morphology, mechanical properties, and free volume.* Macromolecules, 2003. **36**(5): p. 1616-1625.